Journal of Geoscience and Environment Protection, 2026, 14(4), 26-43
https://www.scirp.org/journal/gep
ISSN Online: 2327-4344
ISSN Print: 2327-4336

Analysis of Spatial-Temporal Characteristics of Extreme Precipitation during the Long Rainy Season over East Africa

Niyigena Thadee[1*], Clara Liapapa[1], Sandrine Giramahoro[1], Ebaju Gerverse Kamukama[2]

[1]School of Atmospheric Science, Nanjing University of Information Science and Technology, Nanjing, China
[2]Jiangsu Provincial University Key Laboratory of Agricultural and Ecological Meteorology, School of Ecology and Applied Meteorology, Nanjing University of Information Science and Technology, Nanjing, China
Email: *niyigenathadee@gmail.com

How to cite this paper: Thadee, N., Liapapa, C., Giramahoro, S., & Kamukama, E. G. (2026). Analysis of Spatial-Temporal Characteristics of Extreme Precipitation during the Long Rainy Season over East Africa. *Journal of Geoscience and Environment Protection, 14,* 26-43.
https://doi.org/10.4236/gep.2026.144002

Received: March 4, 2026
Accepted: March 28, 2026
Published: March 31, 2026

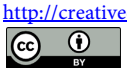

Abstract

In recent decades, rainfall variability across East Africa has intensified, raising concerns regarding the spatial and temporal behavior of extreme precipitation during the long rainy season (March-May). This study analyzes the spatial-temporal characteristics of extreme precipitation over East Africa for the period 1979-2024 using daily precipitation from the ERA5 reanalysis at 0.25˚ resolution. Extreme events are defined using a percentile-based approach that identifies rainfall exceeding the local 90th percentile of wet days. The results reveal pronounced spatial heterogeneity in extreme-event frequency, with western and central sectors experiencing approximately 8 - 10 extreme days per season, while northeastern areas generally record fewer than 3 - 4 days. In contrast, extreme-event intensity exhibits more localized maxima, with median rainfall on extreme days typically ranging between 15 and 30 mm per day and isolated regions exceeding 40 - 60 mm per day. Interannual variability analysis shows that extreme precipitation during March-May is dominated by a coherent large-scale mode explaining roughly one-third of the total variance, indicating organized regional-scale atmospheric control. These findings demonstrate that long rainy season extremes are characterized by systematic spatial gradients, distinct frequency-intensity structures, and structured year-to-year variability. By separating event occurrence from rainfall magnitude and quantifying dominant variability patterns, this study provides an improved characterization of extreme precipitation dynamics during the long rainy season over East Africa.

Keywords

Extreme Precipitation, Spatial-Temporal Variability, East Africa, Long Rainy

Season (MAM)

1. Introduction

In recent decades, climate variability and climate change have increasingly manifested through changes in the characteristics of hydro-meteorological events, particularly rainfall variability and extremes. Alterations in rainfall intensity, frequency, and temporal organization have been observed in many regions of the world, contributing to an increased occurrence of floods, landslides, and water-related hazards. These impacts are often driven more by extreme precipitation events than by changes in mean climate conditions, as short-duration intense rainfall can produce disproportionate socio-economic and environmental consequences (Trenberth et al., 2003; Allan & Soden, 2008).

Africa is especially sensitive to such changes because of its strong dependence on rainfall-driven systems, including rain-fed agriculture, surface water resources, and climate-sensitive livelihoods. Rainfall over the continent exhibits pronounced spatial and temporal variability, shaped by interactions among large-scale atmospheric circulation, land-atmosphere feedbacks, and ocean-atmosphere coupling (Nicholson, 2017; Camberlin, 2018). As a result, both rainfall deficits and excesses have contributed to recurrent droughts and floods, undermining food security and socio-economic stability across many parts of Africa (Reed et al., 2022).

Within Africa, East Africa represents a region of particularly complex hydroclimatic behavior. Rainfall variability is influenced by heterogeneous topography, including the highlands and rift systems, as well as by large inland water bodies such as Lake Victoria. These regional features interact with atmospheric circulation to generate strong seasonal contrasts and substantial interannual variability in rainfall (Indeje et al., 2000). The present study focuses on five countries—Rwanda, Burundi, Uganda, Kenya, and Tanzania—which together form a climatically diverse and socio-economically vulnerable sub-region within East Africa. Much of this region experiences a bimodal rainfall regime, with the long rainy season occurring during March-May (MAM) and the short rainy season during October-December (OND) (Conway et al., 2005). The MAM season is particularly critical, as it provides a major share of annual rainfall and underpins agricultural production, water availability, and ecosystem functioning across these countries (Camberlin & Philippon, 2002; Palmer et al., 2023).

Despite its importance, the long rainy season has exhibited marked variability and periods of rainfall suppression in recent decades, contributing to agricultural stress and food insecurity in the region (Lyon & DeWitt, 2012; Funk et al., 2018). At the same time, intense rainfall episodes during MAM have triggered damaging floods and landslides, especially in topographically complex and densely populated areas. These contrasting impacts highlight the need to better understand not only seasonal rainfall amounts but also the behavior of extreme precipitation dur-

ing the long rainy season.

Previous research on East African rainfall has largely emphasized seasonal totals, interannual variability, and large-scale climatic influences, with particular attention given to the short rainy season. Numerous studies have investigated the role of regional circulation and remote climate drivers in shaping rainfall variability, providing valuable insights into the mechanisms governing seasonal precipitation (Saji et al., 1999; Nicholson, 2017). However, the long rainy season remains comparatively less well understood, as it exhibits weaker and more complex variability and is more difficult to predict than the short rains (Wainwright et al., 2019).

Moreover, much of the existing literature has focused on mean rainfall behavior, while extreme precipitation events—often responsible for the most severe impacts—have received less systematic attention. Changes in extreme rainfall can occur independently of changes in mean precipitation, and analyses based solely on seasonal totals may therefore underestimate climate-related risks (Alexander et al., 2006; Donat et al., 2016). Although percentile-based indices provide a robust framework for identifying precipitation extremes, their application to the long rainy season over East Africa, particularly at sub-regional scales and with explicit consideration of intra-seasonal variability from March to May, remains limited. A focused examination of extreme precipitation during the long rainy season (MAM) is therefore necessary to improve understanding of hydro-climatic variability in East Africa. In particular, there remains limited knowledge of the spatial distribution of extreme precipitation, its intra-seasonal evolution from March to May, and its dominant modes of interannual variability. Addressing these aspects provides insight into the physical behavior of extreme rainfall during the long rains and helps clarify how variability at different temporal and spatial scales contributes to the occurrence of extreme precipitation events.

2. Study Area and Data

East Africa is examined over the period 1979-2024. The study domain covers the East African region bounded by 12˚S-5˚N and 28.5˚E-42˚E, encompassing Rwanda, Burundi, Uganda, Kenya, and Tanzania. This region represents the core area influenced by the March-May long rainy season (**Figure 1**). The region is characterized by complex physiographic features, including elevated highlands, the East African Rift System, interior plateau regions, and coastal lowlands. These topographic variations strongly modulate regional atmospheric circulation, moisture transport, and convection, resulting in substantial spatial heterogeneity in rainfall distribution across relatively short distances. Orographic lifting over highland areas and differential heating between land and adjacent water bodies further contribute to localized rainfall contrasts.

Climatologically, East Africa exhibits a predominantly bimodal rainfall regime associated with seasonal shifts of the Intertropical Convergence Zone (ITCZ). The long rainy season occurs during MAM, followed by a secondary rainfall peak dur-

ing OND. The MAM season accounts for a significant proportion of annual rainfall over much of the region and plays a central role in regional hydrology and water resource availability. Notably, the long rainy season is characterized by pronounced interannual fluctuations in rainfall amount and spatial extent, making it a key period for examining variability and extremes.

To characterize precipitation variability across East Africa, daily precipitation data are derived from the ERA5 (ECMWF Reanalysis v5) reanalysis produced by the European Centre for Medium-Range Weather Forecasts. ERA5 provides a physically consistent reconstruction of the atmospheric state through advanced data assimilation techniques that integrate satellite and in situ observations within a modern numerical weather prediction system. The dataset offers daily precipitation at a spatial resolution of 0.25˚ × 0.25˚, enabling detailed regional-scale assessment of rainfall variability. Also, U and V wind components and Specific humidity are obtained from ERA5.

Sea surface temperature (SST) data are obtained from the NOAA Extended Reconstructed Sea Surface Temperature version 6 (ERSSTv6) dataset. ERSSTv6 is a bias-adjusted, monthly global SST product derived from the International Comprehensive Ocean Atmosphere Data Set (ICOADS) and modern satellite observations. Its long-term consistency and broad spatial coverage (2˚ × 2˚) make it ideal for studying large-scale ocean-atmosphere interactions. the multi-decadal coverage from 1979 to 2024 provides a sufficiently long record for evaluating spatial patterns, temporal variability, and long-term characteristics of precipitation during the long rainy season. Previous studies have shown that ERA5 precipitation performs reasonably well in representing rainfall variability over East Africa when compared with observational datasets such as CRU and GPCC (Assamnew & Mengistu Tsidu, 2022).

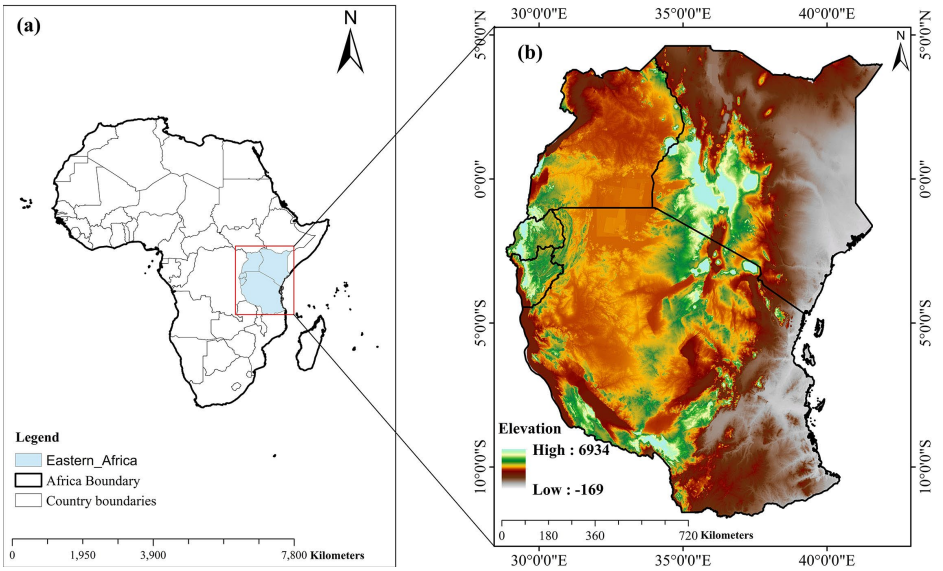

Figure 1. Location and topography of the East African study region. (a) The geographic location of East Africa within the African continent, with the study domain highlighted; (b) Topographic elevation of East Africa.

3. Methods

3.1. Definition of Extreme Precipitation

Extreme precipitation events are defined using a percentile-based threshold calculated independently at each grid point. Wet days are first identified as days with daily precipitation ≥ 1 mm per day. For each grid cell, the 90th percentile (P90) of wet-day precipitation is computed using all available MAM wet days over the analysis period. This procedure produces a spatially varying threshold that reflects the local climatological characteristics of rainfall across the study domain.

3.2. Seasonal Extreme Precipitation Frequency

Seasonal extreme precipitation frequency is quantified for each grid point and each year as the total number of extreme precipitation days occurring during the MAM season. The metric is expressed in units of days per season. Climatological spatial distributions are obtained by averaging seasonal extreme-day frequencies over the entire study period. Regional-scale variability is assessed by spatially averaging grid-point seasonal extreme precipitation frequencies to construct inter-annual time series representing domain-wide variability. Extreme precipitation intensity was defined as the median daily precipitation amount across all extreme days identified at each grid point during the MAM season for the period 1979-2024.

3.3. Intra-Seasonal Variability

To examine intra-seasonal characteristics, extreme precipitation frequency is analyzed separately for March, April, and May. For each month and each year, the number of extreme precipitation days is calculated using the previously defined P90 threshold. Monthly climatological means are subsequently derived to assess the seasonal progression of extreme precipitation within MAM and to evaluate the relative contribution of each month to total seasonal extremes.

3.4. Standardization and Anomaly Construction

To analyze variability relative to the long-term mean state, seasonal extreme precipitation frequency fields are converted into standardized anomaly fields. At each grid point, the climatological mean MAM extreme precipitation frequency over 1979-2024 is subtracted from each annual value to remove the background mean state. The resulting anomaly series is then normalized by its corresponding temporal standard deviation at that grid point. This transformation expresses variability in dimensionless standardized units and enables consistent comparison of spatial-temporal fluctuations across regions characterized by differing climatological magnitudes and variance levels.

3.5. Empirical Orthogonal Function (EOF) Analysis

Empirical Orthogonal Function (EOF) analysis is applied to the standardized sea-

sonal anomaly fields to identify dominant modes of interannual variability in MAM extreme precipitation frequency. Before decomposition, latitude-dependent area weighting is implemented using the square root of the cosine of latitude to account for meridional convergence. The weighted anomaly field is decomposed into orthogonal spatial patterns (EOFs) and corresponding principal components (PCs), which respectively describe the dominant spatial structures and their temporal evolution. The fraction of total variance explained by each EOF mode is calculated to quantify its contribution to overall variability, and the sampling uncertainty of eigenvalues is evaluated following North et al. (1982) to assess the robustness and separability of the leading modes.

3.6. Statistical Test

Long-term trends in MAM extreme precipitation frequency are evaluated at both grid-point and regional scales. The non-parametric Mann-Kendall test is employed to detect monotonic trends over the study period, and trend magnitude is quantified using Sen's slope estimator. Trend magnitudes are expressed in units of days per season per decade, providing a quantitative measure of temporal change in seasonal extreme precipitation frequency.

4. Results

4.1. Seasonal Variability of Extreme Precipitation Frequency

The seasonal evolution of extreme precipitation frequency over East Africa during 1979-2024 reveals marked differences among the four climatological seasons (**Figure 2**). The long rainy season (MAM) exhibits the highest frequency of extreme events throughout the record, generally ranging between approximately 3 and 9 days per season. Notable maxima are observed in the late 1990s and again around 2018, when seasonal counts approach the upper bound of the distribution (**Figure 2(a)**). In contrast, the boreal summer season (JJA) consistently records the lowest frequency, typically remaining below 3 days per season, with limited interannual variability.

The short rainy season (OND) displays moderate variability, with extreme-event frequencies commonly fluctuating between approximately 2 and 8 days per season. DJF exhibits comparable variability but with slightly lower mean values than MAM. Across all seasons, year-to-year fluctuations are evident, indicating substantial interannual variability in extreme-event occurrences.

Seasonal anomaly time series further illustrate departures from the climatological mean (**Figure 2(b)**). Positive MAM anomalies exceeding +3 days are evident during peak years, particularly around 1997-1998 and 2018-2019, while negative anomalies approaching −3 days occur in the early 1980s and early 2000s. OND anomalies show episodic large positive departures exceeding +4 days, whereas JJA anomalies remain comparatively constrained, generally within ±2 days. The amplitude of anomalies confirms that MAM contributes most strongly to seasonal variability in extreme precipitation frequency over the region.

Overall, the results demonstrate that the long rainy season dominates both the mean state and the interannual variability of extreme precipitation frequency across East Africa during the study period.

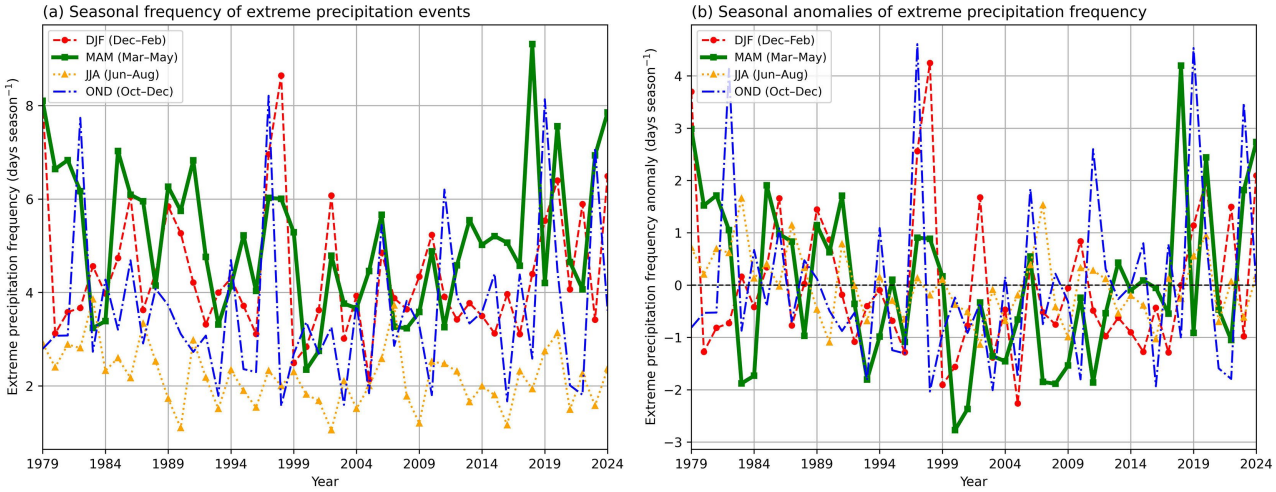

Figure 2. Interannual variability of MAM extreme precipitation frequency averaged over the study region during 1979-2024. (a) Seasonal mean number of extreme days per season; (b) Standardized anomalies of extreme-day frequency relative to the long-term mean.

4.2. Intra-Seasonal Spatial Evolution of MAM Extreme Precipitation

The spatial distribution of mean extreme precipitation frequency exhibits clear intra-seasonal evolution across March, April, and May (**Figure 3**). In March, extreme-event frequency is already established over the western and central portions of the region, with values commonly exceeding 1.5 - 2.5 days per month and localized maxima approaching 3 days per month. In contrast, eastern and northeastern areas display comparatively lower frequencies, generally below 1 day per month.

April represents the peak phase of the long rainy season. Extreme precipitation becomes more widespread and spatially coherent, with large portions of the domain exceeding 2 days per month. The western highlands and central belt exhibit the highest concentrations, locally reaching or surpassing 3 days per month. Compared with March, April shows both an expansion in spatial coverage and an intensification in magnitude, indicating that this month contributes most strongly to the seasonal extreme-event total.

In May, a distinct weakening of extreme precipitation frequency is observed across much of the southern and central areas, where values generally decline to below 1 - 1.5 days per month. However, relatively elevated frequencies persist in parts of the western and northern sectors. The spatial pattern thus reflects a progressive transition from intensification in April to a partial retreat in May, consistent with the typical evolution of the long rainy season.

Overall, the intra-seasonal structure demonstrates that extreme precipitation

during MAM is not uniformly distributed within the season; rather, it intensifies from March to April and subsequently weakens in May, with persistent spatial contrasts between the western/central and eastern portions of the region.

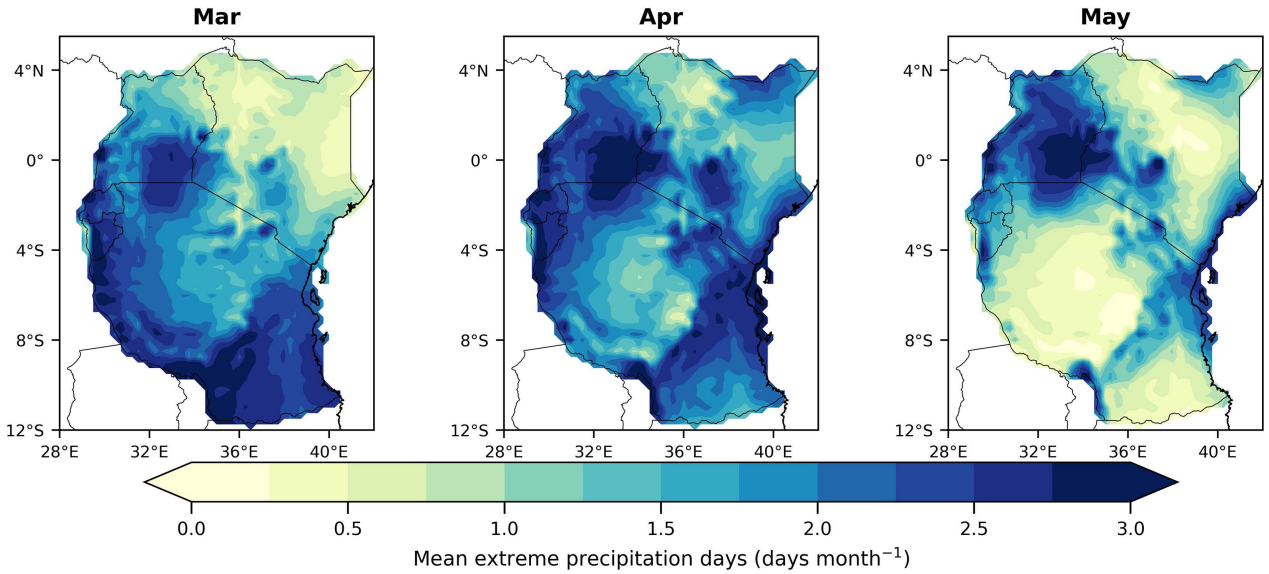

Figure 3. Spatial distribution of the mean number of extreme precipitation days per month for March, April, and May over East Africa. Values represent climatological averages (1979-2024) expressed as days per month, based on the 90th percentile threshold of wet-day precipitation (≥1 mm per day) at each grid point.

4.3. Spatial Characteristics of MAM Extreme Precipitation Frequency and Intensity

The spatial distribution of MAM extreme precipitation exhibits pronounced heterogeneity in both frequency and intensity (**Figure 4**). The seasonal frequency of extreme events (**Figure 4(a)**) indicates that several areas experience between 6 and 10 extreme days per season. The highest frequencies are concentrated over the western and northwestern sectors, where values exceed 8 - 9 days per season. Elevated frequencies are also evident across parts of the central and southeastern zones. In contrast, comparatively lower frequencies, generally below 3 - 4 days per season, are observed in portions of the northeastern interior. Overall, the spatial pattern reveals a clear west-east contrast in the occurrence of extreme precipitation events during the long rainy season.

The spatial distribution of extreme precipitation intensity (**Figure 4(b)**), represented by the median rainfall amount on extreme days, displays a different spatial configuration. Across much of the domain, median intensities range approximately between 15 and 30 mm per day. Localized maxima exceeding 40 - 60 mm per day are observed in discrete areas, particularly over elevated terrain and selected interior zones. In contrast, lower median intensities are found in several northeastern and interior regions. The spatial alignment of intensity maxima does not fully correspond with areas of highest event frequency.

Together, these results demonstrate that the spatial patterns of MAM extreme

precipitation differ between frequency and intensity fields. While the frequency field shows relatively broad regional structures, the intensity field is characterized by more localized variability. These findings demonstrate the spatial characteristics of extreme precipitation during the long rainy season across the study domain.

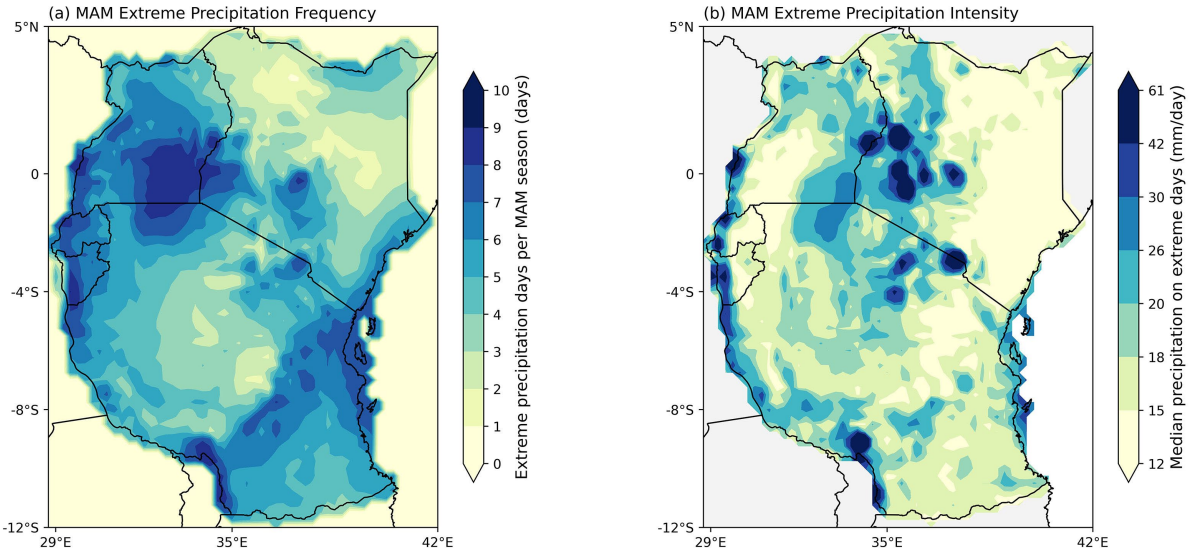

Figure 4. Spatial distribution of MAM extreme precipitation (1979-2024). (a) Mean frequency of extreme precipitation events during March-May (MAM), expressed as the number of extreme days per season; (b) Median rainfall intensity on extreme days (mm per day).

4.4. Comparison between the 90th vs 95th Percentile

A sensitivity analysis was conducted to evaluate the influence of the percentile threshold used to define extreme precipitation events by comparing results derived from the 90th percentile (P90) and the 95th percentile (P95) thresholds (**Figure 5**). The spatial distribution of extreme precipitation frequency during the MAM season based on the P90 threshold is shown in **Figure 5(a)**, where relatively high frequencies are observed across much of the western and northwestern parts of the region, locally exceeding 7 - 10 extreme precipitation days per season. Moderate frequencies (approximately 4 - 7 days) are distributed across central areas, while lower frequencies are present in parts of the eastern and southern regions. When the stricter P95 threshold is applied, the spatial pattern remains broadly similar, but the frequency of extreme precipitation events decreases across the entire region, generally falling below 5 days per season (**Figure 5(c)**).

The spatial distribution of extreme precipitation intensity also exhibits comparable structures between the two thresholds. For the P90 definition, the median intensity of extreme precipitation events ranges from approximately 18 to over 40 mm per day across most of the region, with localized maxima exceeding 60 mm per day in several central and northern areas (**Figure 5(b)**). Under the P95 threshold, the spatial pattern of intensity remains consistent, but the magnitude of the extreme precipitation intensity increases, with some areas exceeding 80 mm per day (**Figure 5(d)**). Overall, while the application of the higher percentile threshold

reduces the frequency of detected extreme precipitation events, the spatial distribution patterns remain similar, and the intensity of the selected events becomes higher.

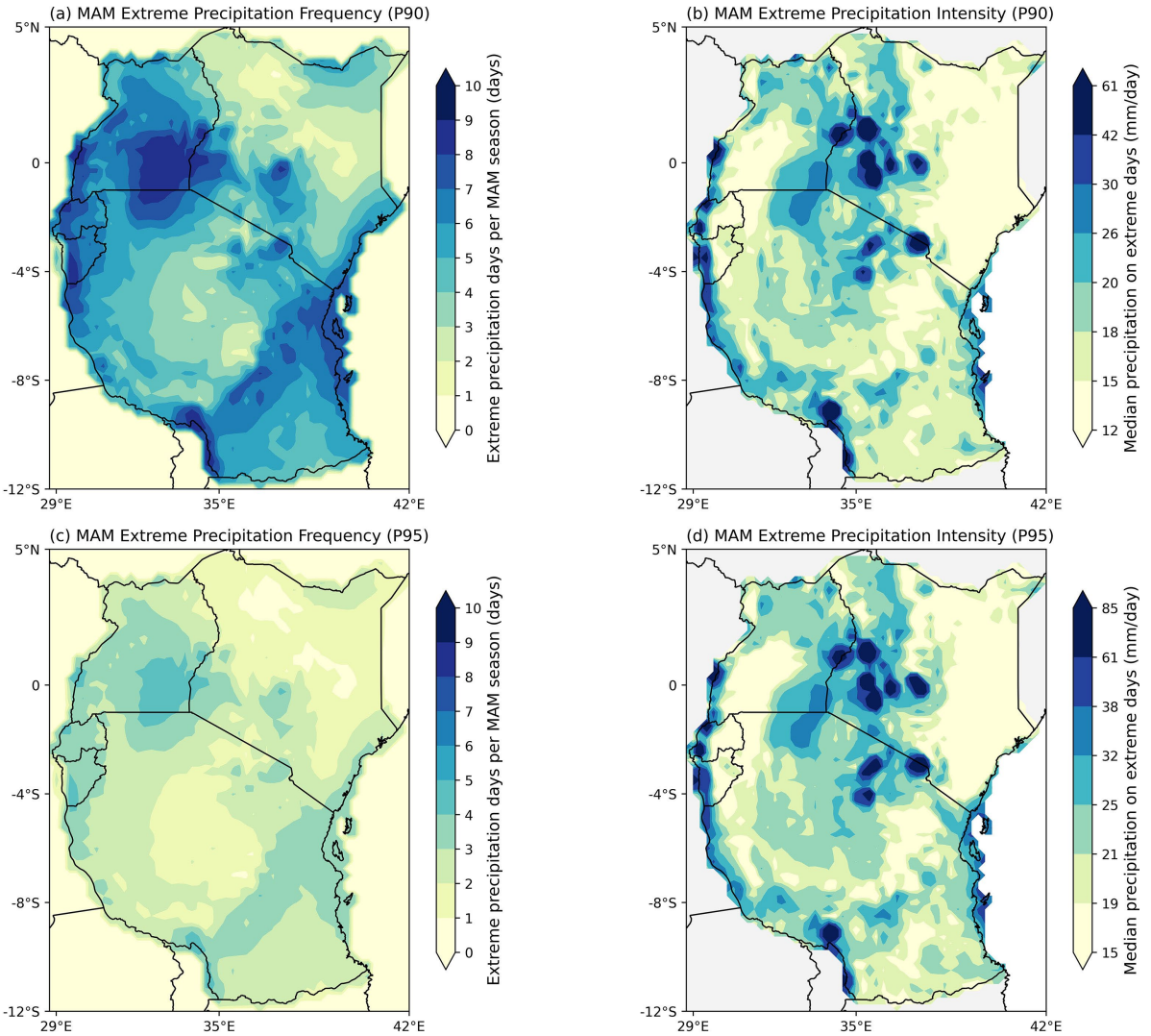

Figure 5. Sensitivity analysis of extreme precipitation characteristics during the March-May (MAM) season using two percentile thresholds. Panels (a) and (b) show the spatial distribution of extreme precipitation frequency (days per season) and median intensity (mm per day) defined using the 90th percentile (P90) of wet-day precipitation, respectively. Panels (c) and (d) present the corresponding results derived from the 95th percentile (P95) threshold.

4.5. Dominant Modes of Interannual Variability of MAM Extreme Precipitation

The leading three EOFs of MAM extreme precipitation frequency together explain 45.6% of the total interannual variance, with EOF1, EOF2, and EOF3 accounting for 31.2%, 8.2%, and 6.2%, respectively (**Figure 6**).

EOF1 (**Figure 6(a)**) represents the dominant mode and exhibits a largely coherent spatial structure across the study domain, with loadings of similar sign over most areas. The associated principal component (PC1; **Figure 6(b)**) displays pronounced

interannual variability, characterized by alternating positive and negative phases throughout the record. Notable positive amplitudes occur during the late 1990s and early 2000s, whereas marked negative values appear in the late 2010s.

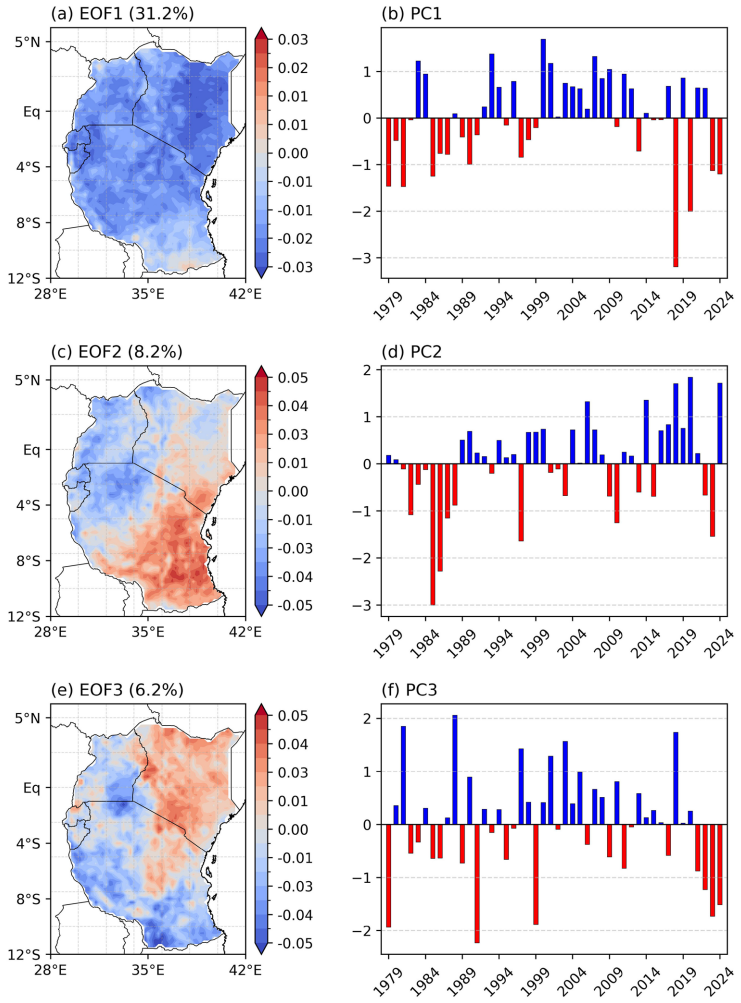

Figure 6. Leading empirical orthogonal functions (EOF1 - EOF3) and the corresponding principal components (PC1~PC3) of standardized MAM extreme precipitation frequency during 1979-2024. Spatial patterns represent EOF loadings, and bar plots show the interannual variability of the associated principal component time series.

EOF2 (**Figure 6(c)**) shows a clear spatial contrast between the southeastern sector and parts of the western and northwestern regions, indicating a dipole-like configuration. Its corresponding time series (PC2; **Figure 6(d)**) reveals strong negative anomalies during the early 1980s and increased positive amplitudes during the 2010s, with intermediate oscillations in between.

EOF3 (**Figure 6(e)**) is characterized by a meridional gradient, with opposing signs between the northern and southern portions of the domain. The associated PC3 (**Figure 6(f)**) demonstrates substantial year-to-year variability, including enhanced positive amplitudes in the late 1980s and early 2000s, and negative excursions toward the end of the record.

Collectively, these modes capture the principal spatial structures governing the interannual variability of extreme precipitation frequency during the long rainy season.

4.6. Physical Drivers

To examine the large-scale ocean-atmosphere conditions associated with the leading mode of extreme precipitation variability, correlations between PC1 of MAM extreme precipitation frequency and global sea surface temperature (SST) anomalies were calculated. The resulting spatial correlation pattern is shown in **Figure 7(a)**. Statistically significant correlations are observed across several tropical ocean basins. In particular, negative correlations appear over parts of the central and eastern tropical Pacific Ocean, while positive correlations are present in portions of the western Pacific and subtropical oceans. Additional significant correlations are evident in the southern Indian Ocean and parts of the extratropical oceans. These SST correlation patterns indicate that the leading mode of extreme precipitation variability over the study region is associated with large-scale oceanic variability across multiple tropical basins.

To further investigate the associated atmospheric circulation, composite anomalies of lower-tropospheric circulation and moisture transport were calculated by subtracting low PC1 years from high PC1 years. The results are shown in **Figure 7(b)**, where shading represents the magnitude of moisture flux anomalies and vectors denote the associated wind anomalies at 850 hPa. The composite pattern reveals pronounced moisture transport anomalies across the tropical belt, particularly over the equatorial Pacific, the Indian Ocean, and parts of the Atlantic Ocean. Enhanced moisture flux anomalies are evident along the tropical convergence zones, indicating strengthened horizontal moisture transport during positive PC1 phases. Over East Africa, the highlighted study region shows notable circulation anomalies accompanied by enhanced moisture transport from the surrounding tropical oceans.

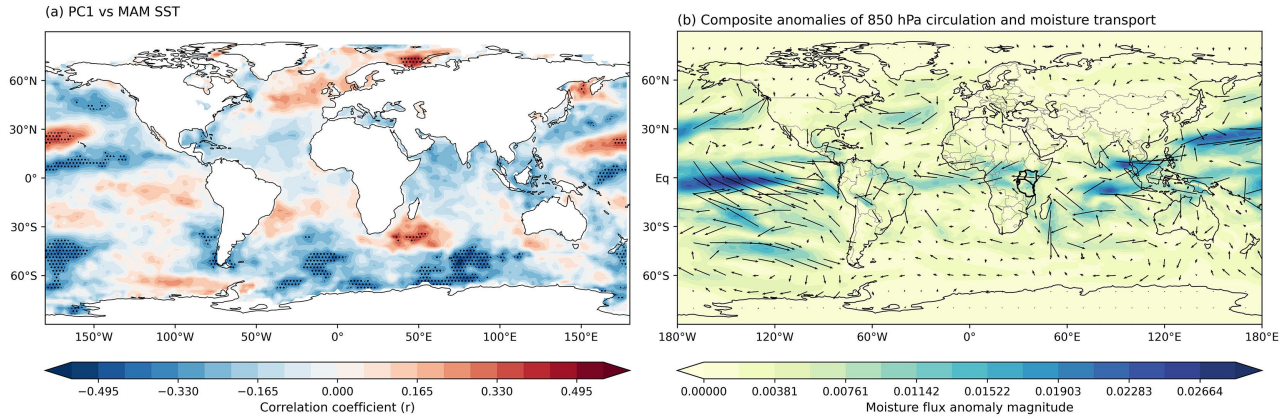

Figure 7. Large-scale Ocean-atmosphere conditions associated with the leading mode of MAM extreme precipitation variability. (a) Spatial correlation between the principal component (PC1) of MAM extreme precipitation frequency and global sea surface temperature (SST) anomalies. Shading indicates the correlation coefficient (r), and stippling denotes statistically significant correlations ($p < 0.05$); (b) Composite anomalies of lower-tropospheric circulation and moisture transport.

5. Discussion

The present analysis provides a quantitatively constrained characterization of extreme precipitation during the long rainy season (MAM) over East Africa, demonstrating that both spatial structure and interannual variability are systematic rather than random. The climatological frequency of extreme events ranges from approximately 3 to 10 days per season across the domain, with western and northwestern sectors exceeding 8 - 9 extreme days per season, compared to fewer than 3 - 4 days in parts of the northeastern interior. This west-east gradient reflects persistent regional asymmetry in moisture convergence and convection during MAM, consistent with previously observed spatial rainfall contrasts over equatorial East Africa (Lyon & DeWitt, 2012; Nicholson, 2017). These results indicate that exposure to extreme rainfall is geographically structured rather than spatially uniform.

In contrast to the relatively coherent spatial structure of extreme-event frequency, the distribution of extreme precipitation intensity exhibits localized maxima, with median rainfall on extreme days commonly between 15 and 30 mm per day and isolated areas exceeding 40 - 60 mm per day. Notably, the regions of highest intensity do not systematically coincide with those of highest frequency. This spatial decoupling suggests that the processes governing event occurrence differ from those controlling rainfall magnitude. While large-scale seasonal circulation likely regulates the number of extreme days, local convective organization and orographic lifting modulate event intensity. Similar distinctions between frequency and intensity drivers have been reported in tropical precipitation studies (Westra et al., 2014; O'Gorman, 2015).

The seasonal migration of the ITCZ provides a fundamental dynamical framework for interpreting the spatial structure observed during MAM. The northward displacement of the ITCZ during boreal spring enhances deep convection and large-scale moisture convergence across equatorial East Africa, influencing both the onset and spatial distribution of long-rain precipitation (Yang et al., 2015; Nicholson, 2018). Variations in the latitudinal position and strength of the ITCZ during MAM can modulate regional rainfall gradients and extreme-event clustering. The pronounced west-east frequency contrast identified here is consistent with differential moisture availability and convergence intensity across the region during this seasonal transition phase.

The interannual variability analysis further reveals substantial year-to-year fluctuations, with seasonal extreme-day counts ranging from below 3 days in dry years to more than 9 days in wet years. The leading EOF mode explains approximately one-third of the total variance, indicating that extreme precipitation variability during MAM is dominated by a coherent regional-scale structure. This magnitude of explained variance confirms that extremes are organized by large-scale atmospheric controls rather than being purely stochastic convective events. Secondary modes contribute smaller but physically interpretable fractions of variability, reflecting subregional differentiation. Comparable dominance of leading

modes in seasonal rainfall variability has been reported for East Africa in prior variability analyses (Lyon & DeWitt, 2012; Funk et al., 2015), although those studies did not explicitly isolate percentile-defined extremes.

Analysis of large-scale ocean-atmosphere conditions associated with the leading precipitation mode further clarifies the physical drivers underlying this variability. Correlations between PC1 and global sea surface temperature anomalies reveal statistically significant relationships across multiple tropical ocean basins, including the Pacific and Indian Oceans. In particular, SST anomalies in the tropical Pacific suggest a linkage with large-scale climate variability associated with the El Niño-Southern Oscillation (ENSO). ENSO-related SST anomalies can influence the Walker circulation and modulate atmospheric convection and precipitation across the tropics, including East Africa (Trenberth et al., 1998; Cai et al., 2014). These teleconnections indicate that variability in remote ocean basins may contribute to the modulation of extreme precipitation during the long rainy season.

The composite analysis of lower-tropospheric circulation and moisture transport further highlights the dynamical mechanisms associated with this variability. During positive phases of the leading EOF mode, enhanced low-level wind anomalies and moisture transport appear along the tropical convergence belt, particularly over the Indian Ocean and equatorial regions. These circulation anomalies indicate strengthened horizontal moisture advection toward East Africa, consistent with enhanced moisture convergence over the region. Such moisture transport pathways are a key component of East African rainfall variability, as the region receives substantial atmospheric moisture from adjacent ocean basins through low-level circulation systems (Saji et al., 1999; Nicholson, 2017). The composite patterns also suggest that shifts in the position and intensity of the tropical convergence zone contribute to the organization of extreme precipitation events during MAM.

These findings refine the understanding of long rainy season extremes by moving beyond seasonal rainfall totals toward percentile-based diagnostics of event occurrence and intensity. Whereas earlier research has emphasized seasonal rainfall variability or drought tendencies (Funk et al., 2015; Nicholson, 2017), the present results demonstrate that extreme precipitation exhibits structured spatial heterogeneity and coherent interannual modes. The clear separation between frequency-dominated and intensity-dominated regions further suggests that infrastructure exposure, hydrological risk, and flood susceptibility may vary spatially in more complex ways than indicated by mean rainfall patterns alone.

Overall, the spatial-temporal characteristics of MAM extreme precipitation revealed here indicate that extremes during the long rainy season are governed by interacting large-scale circulation features and localized amplification mechanisms. The systematic west-east gradient in frequency, the localized concentration of high-intensity events, and the dominance of a primary interannual variability mode together demonstrate that extreme precipitation during MAM is dynamically organized across multiple spatial scales. The additional evidence from SST

correlations and circulation composites further suggests that remote oceanic variability, including ENSO-related processes, and shifts in the ITCZ-related circulation belt play an important role in modulating moisture transport and extreme rainfall variability over East Africa. By quantifying these features within a unified statistical framework, this study contributes to a more resolved understanding of how long-rain extremes are structured in space and time, thereby directly advancing knowledge aligned with the core objective of analyzing the spatial-temporal characteristics of extreme precipitation during the long rainy season over East Africa.

6. Conclusion

This study provides a comprehensive assessment of the spatial-temporal characteristics of extreme precipitation during the long rainy season over East Africa using a percentile-based diagnostic framework. The results demonstrate that MAM extreme precipitation exhibits pronounced spatial heterogeneity, with a persistent west-east gradient in event frequency. Western and central sectors experience approximately 8 - 10 extreme days per season, whereas northeastern areas generally record fewer than 3 - 4 days. In contrast, extreme-event intensity displays more localized maxima, with median rainfall on extreme days typically ranging between 15 and 30 mm per day and isolated regions exceeding 40 - 60 mm per day. The spatial divergence between frequency and intensity indicates that the occurrence and magnitude of extreme rainfall are influenced by partly different physical mechanisms.

The interannual variability of extreme precipitation during MAM is characterized by coherent large-scale organization. The leading empirical orthogonal function explains roughly one-third of the total variance, indicating that seasonal extreme rainfall variability is dominated by structured regional-scale atmospheric processes rather than random convective fluctuations. Secondary modes account for additional but more spatially differentiated variability, reflecting subregional contrasts within the broader seasonal framework. These findings confirm that extremes during the long rainy season are dynamically organized across multiple spatial scales.

Analysis of ocean-atmosphere interactions and atmospheric circulation provides further insight into the physical processes associated with this variability. Correlations between the leading precipitation mode and global sea surface temperature anomalies reveal significant relationships across several tropical ocean basins, including the Pacific and Indian Oceans, suggesting the influence of large-scale climate variability such as ENSO. Composite analysis of lower-tropospheric circulation and moisture transport indicates enhanced horizontal moisture advection toward East Africa during positive phases of the leading variability mode, consistent with shifts in tropical convergence zones and strengthened low-level circulation. These results highlight the role of large-scale atmospheric circulation and moisture transport pathways in modulating extreme precipitation during the

long rainy season.

Overall, the analysis demonstrates that systematic spatial gradients, localized intensity amplification, coherent interannual variability, and large-scale ocean-atmosphere interactions collectively shape MAM extreme precipitation over East Africa. By explicitly separating event frequency from intensity, identifying dominant variability structures, and linking these patterns to large-scale circulation and moisture transport mechanisms, this study advances the understanding of how long rainy season extremes are organized in space and time. The results provide a robust statistical and dynamical foundation for future investigations into the drivers of extreme rainfall and for improving regional assessments of hydroclimatic risk under ongoing climate variability and change.

7. Future Prospective

Despite the advances presented in this study in characterizing the spatial-temporal variability of extreme precipitation during the long rainy season over East Africa, several avenues remain for further investigation. Future research should focus on improving the representation and detection of extreme precipitation events through the integration of multiple observational and satellite-based precipitation products alongside reanalysis datasets. A multi-dataset framework would enable a more comprehensive assessment of uncertainties associated with data resolution, observational coverage, and methodological approaches used in extreme-event identification. Such comparisons would contribute to a more robust regional climatology of rainfall extremes and strengthen confidence in spatial-temporal assessments derived from reanalysis data.

In addition, a deeper understanding of the dynamical mechanisms driving extreme precipitation during the March-May season remains essential. Future studies could explore the role of large-scale atmospheric circulation patterns, including variations in moisture transport, vertical motion, and the seasonal migration of the Intertropical Convergence Zone (ITCZ), in shaping the occurrence and distribution of extreme rainfall events. Combining statistical diagnostics with dynamical analyses and climate model experiments would provide greater insight into the physical processes governing extreme precipitation variability. Such investigations are particularly important for evaluating potential changes in the frequency and intensity of rainfall extremes under evolving climate conditions and for supporting improved climate risk assessment and adaptation planning across East Africa.

Acknowledgements

I acknowledge the Government of Rwanda for providing the opportunity to pursue advanced studies and the Ministry of Commerce of the People's Republic of China (MOFCOM) for financial support. Sincere appreciation is extended to Nanjing University of Information Science and Technology for providing a supportive academic and research environment throughout this study. I also acknowledge the

European Centre for Medium-Range Weather Forecasts (ECMWF) for the ERA5 reanalysis dataset, which ensures open access to essential climate data used in this research.

Conflicts of Interest

There are no conflicts of interest regarding this study.

References

Alexander, L. V., Zhang, X., Peterson, T. C., Caesar, J., Gleason, B., Klein Tank, A. M. G. et al. (2006). Global Observed Changes in Daily Climate Extremes of Temperature and Precipitation. *Journal of Geophysical Research: Atmospheres, 111,* D05109. https://doi.org/10.1029/2005jd006290

Allan, R. P., & Soden, B. J. (2008). Atmospheric Warming and the Amplification of Precipitation Extremes. *Science, 321,* 1481-1484. https://doi.org/10.1126/science.1160787

Assamnew, A. D., & Mengistu Tsidu, G. (2022). Assessing Improvement in the Fifth-Generation ECMWF Atmospheric Reanalysis Precipitation over East Africa. *International Journal of Climatology, 43,* 17-37. https://doi.org/10.1002/joc.7697

Cai, W., Borlace, S., Lengaigne, M., van Rensch, P., Collins, M., Vecchi, G. et al. (2014). Increasing Frequency of Extreme El Niño Events Due to Greenhouse Warming. *Nature Climate Change, 4,* 111-116. https://doi.org/10.1038/nclimate2100

Camberlin, P. (2018). *Climate of Eastern Africa*. Oxford Research Encyclopedia of Climate Science. https://doi.org/10.1093/acrefore/9780190228620.013.512

Camberlin, P., & Philippon, N. (2002). The East African March-May Rainy Season: Associated Atmospheric Dynamics and Predictability over the 1968-97 Period. *Journal of Climate, 15,* 1002-1019. https://doi.org/10.1175/1520-0442(2002)015<1002:teammr>2.0.co;2

Conway, D., Allison, E., Felstead, R., & Goulden, M. (2005). Rainfall Variability in East Africa: Implications for Natural Resources Management and Livelihoods. *Philosophical Transactions of the Royal Society A: Mathematical, Physical and Engineering Sciences, 363,* 49-54. https://doi.org/10.1098/rsta.2004.1475

Donat, M. G., Lowry, A. L., Alexander, L. V., O'Gorman, P. A., & Maher, N. (2016). More Extreme Precipitation in the World's Dry and Wet Regions. *Nature Climate Change, 6,* 508-513. https://doi.org/10.1038/nclimate2941

Funk, C., Harrison, L., Shukla, S., Pomposi, C., Galu, G., Korecha, D. et al. (2018). Examining the Role of Unusually Warm Indo-Pacific Sea-surface Temperatures in Recent African Droughts. *Quarterly Journal of the Royal Meteorological Society, 144,* 360-383. https://doi.org/10.1002/qj.3266

Funk, C., Peterson, P., Landsfeld, M., Pedreros, D., Verdin, J., Shukla, S. et al. (2015). The Climate Hazards Infrared Precipitation with Stations—A New Environmental Record for Monitoring Extremes. *Scientific Data, 2,* Article 150066. https://doi.org/10.1038/sdata.2015.66

Indeje, M., Semazzi, F. H. M., & Ogallo, L. J. (2000). ENSO Signals in East African Rainfall Seasons. *International Journal of Climatology, 20,* 19-46. https://doi.org/10.1002/(sici)1097-0088(200001)20:1<19::aid-joc449>3.0.co;2-0

Lyon, B., & DeWitt, D. G. (2012). A Recent and Abrupt Decline in the East African Long Rains. *Geophysical Research Letters, 39,* L02702. https://doi.org/10.1029/2011gl050337

Nicholson, S. E. (2017). Climate and Climatic Variability of Rainfall over Eastern Africa.

Reviews of Geophysics, 55, 590-635. https://doi.org/10.1002/2016rg000544

Nicholson, S. E. (2018). The ITCZ and the Seasonal Cycle over Equatorial Africa. *Bulletin of the American Meteorological Society, 99,* 337-348. https://doi.org/10.1175/bams-d-16-0287.1

O'Gorman, P. A. (2015). Precipitation Extremes under Climate Change. *Current Climate Change Reports, 1,* 49-59. https://doi.org/10.1007/s40641-015-0009-3

Palmer, P. I., Wainwright, C. M., Dong, B., Maidment, R. I., Wheeler, K. G., Gedney, N. et al. (2023). Drivers and Impacts of Eastern African Rainfall Variability. *Nature Reviews Earth & Environment, 4,* 254-270. https://doi.org/10.1038/s43017-023-00397-x

Reed, C., Anderson, W., Kruczkiewicz, A., Nakamura, J., Gallo, D., Seager, R. et al. (2022). The Impact of Flooding on Food Security across Africa. *Proceedings of the National Academy of Sciences, 119,* e2119399119. https://doi.org/10.1073/pnas.2119399119

Saji, N. H., Goswami, B. N., Vinayachandran, P. N., & Yamagata, T. (1999). A Dipole Mode in the Tropical Indian Ocean. *Nature, 401,* 360-363. https://doi.org/10.1038/43854

Trenberth, K. E., Branstator, G. W., Karoly, D., Kumar, A., Lau, N., & Ropelewski, C. (1998). Progress during TOGA in Understanding and Modeling Global Teleconnections Associated with Tropical Sea Surface Temperatures. *Journal of Geophysical Research: Oceans, 103,* 14291-14324. https://doi.org/10.1029/97jc01444

Trenberth, K. E., Dai, A., Rasmussen, R. M., & Parsons, D. B. (2003). The Changing Character of Precipitation. *Bulletin of the American Meteorological Society, 84,* 1205-1218. https://doi.org/10.1175/bams-84-9-1205

Wainwright, C. M., Marsham, J. H., Keane, R. J., Rowell, D. P., Finney, D. L., Black, E. et al. (2019). 'Eastern African Paradox' Rainfall Decline Due to Shorter Not Less Intense Long Rains. *npj Climate and Atmospheric Science, 2,* Article No. 34. https://doi.org/10.1038/s41612-019-0091-7

Westra, S., Fowler, H. J., Evans, J. P., Alexander, L. V., Berg, P., Johnson, F. et al. (2014). Future Changes to the Intensity and Frequency of Short-Duration Extreme Rainfall. *Reviews of Geophysics, 52,* 522-555. https://doi.org/10.1002/2014rg000464

Yang, W., Seager, R., Cane, M. A., & Lyon, B. (2015). The Annual Cycle of East African Precipitation. *Journal of Climate, 28,* 2385-2404. https://doi.org/10.1175/jcli-d-14-00484.1